ARTICLES

$\Upsilon(1S) \rightarrow \gamma +$ noninteracting particles

R. Balest,[1] K. Cho,[1] W.T. Ford,[1] D.R. Johnson,[1] K. Lingel,[1] M. Lohner,[1] P. Rankin,[1] J.G. Smith,[1] J.P. Alexander,[2] C. Bebek,[2] K. Berkelman,[2] K. Bloom,[2] T.E. Browder,[2,*] D.G. Cassel,[2] H.A. Cho,[2] D.M. Coffman,[2] D.S. Crowcroft,[2] P.S. Drell,[2] D. Dumas,[2] R. Ehrlich,[2] P. Gaidarev,[2] R.S. Galik,[2] M. Garcia-Sciveres,[2] B. Geiser,[2] B. Gittelman,[2] S.W. Gray,[2] D.L. Hartill,[2] B.K. Heltsley,[2] S. Henderson,[2] C.D. Jones,[2] S.L. Jones,[2] J. Kandaswamy,[2] N. Katayama,[2] P.C. Kim,[2] D.L. Kreinick,[2] G.S. Ludwig,[2] J. Masui,[2] J. Mevissen,[2] N.B. Mistry,[2] C.R. Ng,[2] E. Nordberg,[2] J.R. Patterson,[2] D. Peterson,[2] D. Riley,[2] S. Salman,[2] M. Sapper,[2] F. Würthwein,[2] M.M. Urish,[2] P. Avery,[3] A. Freyberger,[3] J. Rodriguez,[3] S. Yang,[3] J. Yelton,[3] D. Cinabro,[4] T. Liu,[4] M. Saulnier,[4] R. Wilson,[4] H. Yamamoto,[4] T. Bergfeld,[5] B.I. Eisenstein,[5] G. Gollin,[5] B. Ong,[5] M. Palmer,[5] M. Selen,[5] J.J. Thaler,[5] K.W. Edwards,[6] M. Ogg,[6] A. Bellerive,[7] D.I. Britton,[7] E.R.F. Hyatt,[7] D.B. MacFarlane,[7] P.M. Patel,[7] B. Spaan,[7] A.J. Sadoff,[8] R. Ammar,[9] P. Baringer,[9] A. Bean,[9] D. Besson,[9] D. Coppage,[9] N. Copty,[9] R. Davis,[9] N. Hancock,[9] M. Kelly,[9] S. Kotov,[9] I. Kravchenko,[9] N. Kwak,[9] H. Lam,[9] Y. Kubota,[10] M. Lattery,[10] M. Momayezi,[10] J.K. Nelson,[10] S. Patton,[10] R. Poling,[10] V. Savinov,[10] S. Schrenk,[10] R. Wang,[10] M.S. Alam,[11] I.J. Kim,[11] Z. Ling,[11] A.H. Mahmood,[11] J.J. O'Neill,[11] H. Severini,[11] C.R. Sun,[11] F. Wappler,[11] G. Crawford,[12] C. M. Daubenmier,[12] R. Fulton,[12] D. Fujino,[12] K.K. Gan,[12] K. Honscheid,[12] H. Kagan,[12] R. Kass,[12] J. Lee,[12] R. Malchow,[12] M. Sung,[12] C. White,[12] M.M. Zoeller,[12] F. Butler,[13] X. Fu,[13] B. Nemati,[13] W.R. Ross,[13] P. Skubic,[13] M. Wood,[13] M. Bishai,[14] J. Fast,[14] E. Gerndt,[14] R.L. McIlwain,[14] T. Miao,[14] D.H. Miller,[14] M. Modesitt,[14] D. Payne,[14] E.I. Shibata,[14] I.P.J. Shipsey,[14] P.N. Wang,[14] M. Battle,[15] J. Ernst,[15] L. Gibbons,[15] Y. Kwon,[15] S. Roberts,[15] E.H. Thorndike,[15] C.H. Wang,[15] J. Dominick,[16] M. Lambrecht,[16] S. Sanghera,[16] V. Shelkov,[16] T. Skwarnicki,[16] R. Stroynowski,[16] I. Volobouev,[16] G. Wei,[16] P. Zadorozhny,[16] M. Artuso,[17] M. Gao,[17] M. Goldberg,[17] D. He,[17] N. Horwitz,[17] G.C. Moneti,[17] R. Mountain,[17] F. Muheim,[17] Y. Mukhin,[17] S. Playfer,[17] Y. Rozen,[17] S. Stone,[17] X. Xing,[17] G. Zhu,[17] J. Bartelt,[18] S.E. Csorna,[18] Z. Egyed,[18] V. Jain,[18] D. Gibaut,[19] K. Kinoshita,[19] P. Pomianowski,[19] B. Barish,[20] M. Chadha,[20] S. Chan,[20] D.F. Cowen,[20] G. Eigen,[20] J.S. Miller,[20] C. O'Grady,[20] J. Urheim,[20] A.J. Weinstein,[20] M. Athanas,[21] W. Brower,[21] G. Masek,[21] H.P. Paar,[21] M. Sivertz,[21] J. Gronberg,[22] R. Kutschke,[22] S. Menary,[22] R.J. Morrison,[22] S. Nakanishi,[22] H.N. Nelson,[22] T.K. Nelson,[22] C. Qiao,[22] J.D. Richman,[22] A. Ryd,[22] D. Sperka,[22] H. Tajima,[22] and M.S. Witherell[22]

(CLEO Collaboration)

[1] *University of Colorado, Boulder, Colorado 80309-0390*
[2] *Cornell University, Ithaca, New York 14853*
[3] *University of Florida, Gainesville, Florida 32611*
[4] *Harvard University, Cambridge, Massachusetts 02138*
[5] *University of Illinois, Champaign-Urbana, Illinois 61801*
[6] *Carleton University, Ottawa, Ontario K1S 5B6 and the Institute of Particle Physics, Canada*
[7] *McGill University, Montréal, Québec H3A 2T8 and the Institute of Particle Physics, Canada*
[8] *Ithaca College, Ithaca, New York 14850*
[9] *University of Kansas, Lawrence, Kansas 66045*
[10] *University of Minnesota, Minneapolis, Minnesota 55455*
[11] *State University of New York at Albany, Albany, New York 12222*
[12] *Ohio State University, Columbus, Ohio 43210*
[13] *University of Oklahoma, Norman, Oklahoma 73019*
[14] *Purdue University, West Lafayette, Indiana 47907*
[15] *University of Rochester, Rochester, New York 14627*
[16] *Southern Methodist University, Dallas, Texas 75275*
[17] *Syracuse University, Syracuse, New York 13244*
[18] *Vanderbilt University, Nashville, Tennessee 37235*
[19] *Virginia Polytechnic Institute and State University, Blacksburg, Virginia 24061*
[20] *California Institute of Technology, Pasadena, California 91125*
[21] *University of California, San Diego, La Jolla, California 92093*
[22] *University of California, Santa Barbara, California 93106*

(Received 11 August 1994)

*Permanent address: University of Hawaii at Manoa.

We consider the decay of $\Upsilon(1S)$ particles produced at CESR into a photon which is observed by the CLEO detector plus particles which are not seen. These could be real particles which fall outside of our acceptance, or particles which are noninteracting. We report the results of our search for the process $\Upsilon(1S) \to \gamma$ + "unseen" for photon energies >1 GeV, obtaining limits for the case where "unseen" is either a single particle or a particle-antiparticle pair. Our upper limits represent the highest sensitivity measurements for such decays to date.

PACS number(s): 13.40.Hq, 14.40.Gx, 14.80.−j

I. INTRODUCTION

The radiative decays of heavy quarkonia (J/ψ and Υ) offer an opportunity to search for many exotic particles, both within the standard model (Higgs bosons [1,2] or glueballs) as well as beyond the standard model [axions [3,1,2,4], cosmions [5,6], and supersymmetric and other weakly interacting massive particles ("WIMP"'s) [7]]. For the latter class, the couplings of some of these exotic particles with ordinary matter may be sufficiently weak as to leave no detectable trace in a conventional particle detector. The signature for such exotic radiative decays would therefore be the observation of only a single photon in a detector, with considerable missing energy and momentum.

In some of these cases, such as for axions, the coupling of the undetected particle to quarks can vary with quark species. For the "standard" axion a_0 in a two Higgs doublet model, the axion–heavy-quark couplings are prescribed by a single parameter x, defined as the ratio of the the vacuum expectation values of the neutral Higgs fields. For quarkonia decaying radiatively via $q\bar{q} \to \gamma + a_0$, the dependence of decay rate on x is proportional to $x^2(x^{-2})$ for charge 2/3(-1/3) constituent quarks. Hence, the product of the decay widths $\Gamma(J/\psi \to \gamma + a_0) \times \Gamma(\Upsilon \to \gamma + a_0)$ is independent of x. Based on this, the standard axion has been ruled out by the combined results of radiative ψ and radiative Υ decay [1,8].

The formalism of quark-axion couplings can be extended to other particles, and, in particular, to light spin-1 neutral gauge bosons. For example, in the same way that there is a U(1) vector gauge boson related to conservation of electric charge, that there may be other U(1) gauge bosons related to the conservation of baryon or lepton number [9,10]. Such a boson could, in principle, effect a neutral current which would be purely vectorial in the simplest case of a single Higgs doublet. However, if there is more than one Higgs doublet (as required by supersymmetric extensions of the standard model), such a current may in general have an axial vector component as well as a vectorial one. The corresponding neutral gauge boson would then acquire, through its axial vector couplings, effective couplings to quarkonia reproducing those of an axion, and could be produced directly in radiative quarkonium decays. The effective coupling strength of the new gauge boson to quarkonia would reproduce that of a standard axion, but modified by a parameter r, fixed by the ratio of the electroweak scale (0.25 TeV) to the U(1) symmetry-breaking scale. The present Crystal Ball limit on $\Upsilon(1S) \to \gamma + X$ implies that the coupling parameter r should satisfy $r^2 \leq 1/2$; i.e., the scale of U(1) symmetry breaking is slightly above the electroweak scale.

We present in this paper the result of a search for $\Upsilon(1S)$ decays into a photon plus stable [11], noninteracting particles ("X") using the CLEO-II detector at the Cornell Electron Storage Ring. The scope of the search encompasses both two-body ($\Upsilon \to \gamma X$) as well as three-body ($\Upsilon \to \gamma \bar{X} X$) radiative decays. Both the Crystal Ball and ARGUS Collaborations have done searches for such decays; the most stringent limit to date on undetected, long-lived particles produced in two-body radiative Υ decay is the upper limit of $\sim 5 \times 10^{-5}$ on the branching fraction set by the Crystal Ball Collaboration [1].

II. DETECTOR, DATA SAMPLE, AND EVENT SELECTION

The CLEO-II detector is a general purpose solenoidal magnetic spectrometer and calorimeter. Elements of the detector and performance characteristics are described in detail elsewhere [12]. The detector is designed to have high efficiency for triggering and reconstruction of both low-multiplicity as well as high-multiplicity e^+e^- annihilation events. Charged particle momentum measurements are made with three nested cylindrical drift chambers, consisting of 6, 10, and 51 layers of sense wires, respectively. These chambers fill the volume $r = 4.5$ cm to $r = 92$ cm, where r is the radial coordinate relative to the beam axis. Outside the central tracking chambers are plastic scintillation counters which are used as a fast element in the trigger system and also give particle identification information from time of flight measurements. Beyond the time of flight system is the electromagnetic calorimeter, consisting of 7800 thallium-doped CsI crystals. This crystal array gives energy resolution of approximately 4% at 100 MeV, and 1.2% at 5 GeV. The central "barrel" region of the detector covers roughly 80% of the full solid angle. The end-cap regions extend the solid angle coverage of the calorimeter to 95% of 4π, albeit with poorer energy resolution than the barrel region. The entire CsI array is subdivided into blocks (16 in the barrel) for triggering purposes; each block is attached to two discriminators. The "low-energy" discriminator turns on a bit in the trigger logic if 100 MeV< E <500 MeV is deposited in that trigger block; the "high-energy" discriminator has a threshold corresponding to >500 MeV deposited.

The tracking system, time of flight counters, and calorimeter are contained within a 1.5 T superconducting coil. Flux return and tracking chambers used for muon detection are located immediately outside the coil, in an octagonal geometry, and also in the two end-cap regions.

A. Data sample and event selection

This study examines events taken on the peak of the $\Upsilon(1S)$ resonance in 1992, comprising 48 pb^{-1} of integrated luminosity and corresponding to approximately 960 000 $\Upsilon(1S)$ decays. A special trigger was installed for the $\Upsilon(1S)$ data taking for this study. The trigger line ran at approximately 8 Hz during the data taking; additional cuts were employed in our on-line software to suppress backgrounds due to cosmic rays and thereby reduce by a factor of 4 the amount of data actually written to tape from this trigger line. Off-line software filters were then applied to further suppress backgrounds. The same trigger conditions as those used for the direct photon search at the $\Upsilon(1S)$ energy were also used during runs preceding the $\Upsilon(1S)$ data taking, when we took data at continuum center of mass energies about 1 GeV above the $\Upsilon(1S)$. This off-resonance data set is then used for background studies.

The efficiencies of all the hardware and software selection requirements imposed on our sample are evaluated directly from the data, using $e^+e^- \rightarrow \gamma\gamma$, $e^+e^- \rightarrow e^+e^-\gamma$, $e^+e^- \rightarrow \mu^+\mu^-$ events and random trigger events taken from the same data set.

The cuts imposed, as well as their calculated efficiencies [13], are as follows.

At the trigger level, we demand that there be minimal activity in the trigger lines designed to fire if charged tracks are present ($\epsilon = 98.8 \pm 0.1\%$) [14] and there be exactly one "high-energy" trigger bit set in the barrel calorimeter (i.e., deposited energy in a single trigger block exceeding 500 MeV). We designate E_γ as the energy of the shower which fired this trigger bit. Owing to this trigger requirement, this shower also corresponds to the maximum energy shower in the event. Requiring that there be "exactly" one such shower means that we demand that there be no other 500 MeV trigger bits set in the end cap and no other 100 or 500 MeV trigger bits set in the barrel. The trigger cut is purposely looser in the end cap to allow for the higher backgrounds in the forward regions of the detector. Based on a sample of photons which have already satisfied all the other cuts enumerated above, the net efficiency of these calorimeter-based trigger requirements has an energy dependence $F(E_\gamma)$, displayed in Fig. 1, which has been determined using $\gamma\gamma$ and $e^+e^-\gamma$ events [15]. Some of the inefficiency reflected in this curve arises from cases where the shower is not well contained in one of the 16 crystal trigger blocks of the calorimeter (8 segments in $\phi \times$ 2 segments in z). Energy leakage into an adjacent block can then fire the trigger in that neighboring block. Note that this also introduces a position dependence of the efficiency, e.g., an 800 MeV shower which is pointed at the boundary between two trigger blocks may fail to fire the high-energy discriminator in either block if the deposited energy is distributed equally between them.

A total of 6.56×10^6 events in the $\Upsilon(1S)$ data set satisfied these trigger requirements.

On-line software filtering demands that there be a low muon chamber occupancy, consistent with single photons and inconsistent with cosmic rays ($\epsilon = 99.9 \pm 0.03\%$) and

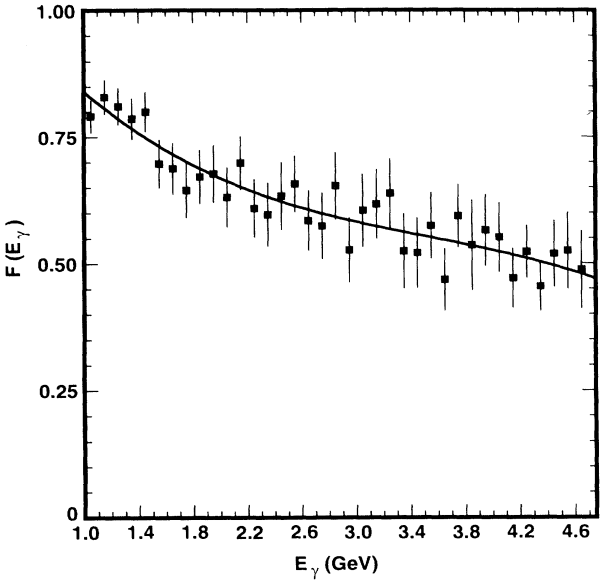

FIG. 1. Efficiency $F(E_\gamma)$ as a function of candidate photon energy for a barrel photon to set exactly one barrel calorimeter trigger bit.

the ratio of energy deposited in the four central crystals of the shower with energy E_γ relative to all the energy deposited in the barrel calorimeter ($E^{\rm tot}_{\rm shower}$) exceeds 0.75; and that the ratio of energy deposited in the nine central crystals of this shower relative to $E^{\rm tot}_{\rm shower}$ exceeds 0.80 ($\epsilon = 97.1 \pm 0.2\%$ for $E_\gamma > 1.5$ GeV; below 1.5 GeV, the efficiency falls slowly to a value of 0.75 at $E_\gamma = 1.0$ GeV as the ambient noise level becomes a larger fraction of the total calorimeter energy).

There were a total of 8.6×10^5 events written to tape which satisfied both the trigger as well as the on-line filter requirements.

Off-line software cuts imposed to reject cosmic rays demand that the event not have hits concentrated in one octant of the muon chambers, and hits in the muon chambers not extrapolate to make a match with the most energetic shower in the calorimeter.

These cosmic ray rejection criteria have a measured efficiency of $96.0 \pm 0.2\%$.

Off-line selection of single photon events demands the following.

The lateral shower shape of the candidate photon is consistent with real photons ($\epsilon = 89.3 \pm 0.2\%$).

A stronger restriction on the amount of excess calorimeter activity than that allowed at the trigger level. In particular, we require that the difference ($E^{\rm tot}_{\rm shower} - E_\gamma$) < 70 MeV ($\epsilon = 85.0 \pm 0.4\%$).

The shower with energy E_γ is confined within the "good" barrel region $|\cos\theta_\gamma| < 0.7$, where θ_γ is the polar angle of the shower with respect to the beam axis.

The shower is not in a region of the calorimeter known to be subject to spurious electronic noise ($\epsilon = 98.8 \pm 0.1\%$).

For single photon events already contained in the "good" barrel region of the calorimeter, taking into ac-

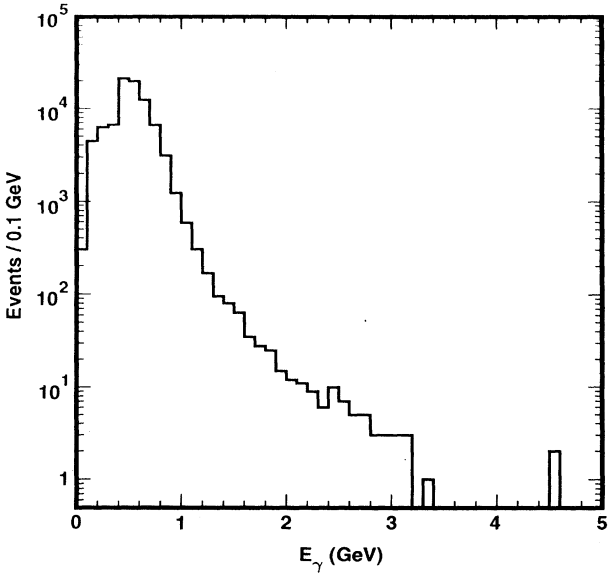

FIG. 2. dN/dE_γ for events passing filter cuts.

count the correlations between all the cuts imposed, the total event efficiency is thus calculated from the data to be about 39%. This is approximately the product of the efficiency function $F(E_\gamma)$ shown in Fig. 1 and the effect of the other cuts enumerated above which we use to define our candidate event sample. By comparison, the efficiency as calculated from a full GEANT-based Monte Carlo simulation of the CLEO detector for the radiative decays of interest, including simulation of all trigger efficiencies, is about 2% (absolute) higher than the value we derive from data. The Monte Carlo and data efficiencies therefore agree to within 5% relative to one other.

After imposing all the above requirements, we have suppressed 92.3% of the single photon candidates that were written to tape. Roughly 8.4×10^4 events are left for further analysis. Figure 2 shows the E_γ spectrum for these remaining events.

Since background processes tend to produce low energy showers, we require that, for further consideration as a candidate signal photon, the most energetic shower have energy in excess of 1 GeV. This photon energy cutoff implies that the maximum mass of X from the three-body process $[\Upsilon(1S) \to \gamma + X\bar{X}]$ to which we are sensitive in this study is 4.20 GeV, and that our sensitivity for the two-body case $[\Upsilon(1S) \to \gamma + X]$ corresponds to $0.0 < M_X < 8.40$ GeV [16].

III. EVALUATION OF BACKGROUNDS

Aside from the process of interest, there are at least three background processes which we expect to contribute to our candidate event sample. These are cosmic ray backgrounds, backgrounds due to single-beam interactions (e.g., beam wall and beam gas), and QED backgrounds. These processes give showers with quite distinct angular distributions in the detector, and quite different energy spectra.

Cosmic rays which have not yet been rejected by our other cuts are characterized by a multitude of predominantly low-energy clusters in the calorimeter which tend to be aligned along the vertical axis. Such background events are independent of any beam conditions, and depend only on exposure time.

Single beam related backgrounds are characterized by energy depositions primarily at forward angles with respect to the beam axis. Along the horizontal ($\phi = 0$ and $\phi = \pi$), the dispersions in beam size and particle energy, as well as the magnitude of synchrotron radiation, are considerably larger than those along the vertical axis. Correspondingly, such events should primarily populate the horizontal plane in azimuth. Such single-beam backgrounds depend not on the e^+e^- collision luminosity, but on the integrated charge passing through the interaction point (i.e., the single-beam currents). Beam-gas or beam-wall collisions produce observed E_γ energy depositions which increase logarithmically with increasing beam energy; photon backgrounds due to beam straggle or single-beam radiation scale directly as energy.

QED backgrounds will arise from $e^+e^- \to e^+e^-\gamma$ and higher order processes. This background could be due, e.g., to cases where the incident leptons lose some of their energy to a high p_T photon, and emerge with too little transverse momentum to be found within the fiducial volume of the detector. Also possible are cases where a lepton scatters into the fiducial volume of CLEO, but is undetected as a charged track [17]. Assuming no beam polarization in CESR, the resulting shower energy spectrum from QED processes will be isotropic in azimuth, but strongly forward peaked in polar angle. The production cross section of such QED backgrounds will scale with luminosity and have an energy dependence as $1/s$. We expect the raw energy distribution for such backgrounds to scale with $E_{\rm beam}$.

The total background from all sources will therefore have some rather complicated dependence on beam energy, beam currents, and CESR luminosity.

Backgrounds are assessed differently in two distinct shower energy regimes. For $1.0 < E_\gamma < 1.5$ GeV, the event count is prohibitively large for scanning, and a statistical subtraction procedure is followed using data taken off the $\Upsilon(1S)$ resonance. These data can then be used as a background sample in evaluating our $1.0 < E_\gamma < 1.5$ GeV signal. However, the unknown fractions of the three types of backgrounds make it difficult to know *a priori* the proper scale factor to use for the continuum sample. We therefore use an empirical scale factor which is obtained from the data itself, by determining the scale factor required to match the continuum sample to the $\Upsilon(1S)$ sample in the "sideband" photon energy region ($0.5 < E_\gamma < 1.0$ GeV), below the signal region.

Comparing the event yields for the on- vs off-resonance data samples, we find that the scale factor needed to saturate the on-resonance photon spectrum with the off-resonance spectrum in the sideband region is approximately equal to the scale factor that we would calculate if we assumed that the only source of background is from

single-beam backgrounds. This is consistent with the interpretation that single-beam effects represent the dominant background in this E_γ region [18]. In this case, we expect the distributions to be more similar in scaled, rather than absolute energy. We therefore perform our subtraction in the simple scale variable z $(= E_\gamma/E_{\rm beam})$ rather than E_γ, normalizing the continuum data to the $\Upsilon(1S)$ data in the sideband interval $(0.12 < z < 0.20)$ [19]. We then apply this scale factor to the signal region $(0.2 < z < 0.3)$, and perform the subtraction. The resulting continuum-subtracted z spectrum is then converted back to E_γ by scaling by $E_{\rm beam}$, and retained as our candidate signal spectrum for the low photon energy interval.

As a check on the procedure, we have compared the characteristics of the photons selected from the $\Upsilon(1S)$ and continuum data sets. The $\Upsilon(1S)$ and continuum samples show good agreement in the shape of their z spectra. Figure 3 shows the comparison of most energetic shower energy between our resonant data sample and our background data sample after all cuts have been applied (as described above, the two plots have been normalized in the photon energy region below 1.0 GeV). Another notable similarity is found between the $\cos\theta_\gamma$ distributions of the two samples after all cuts have been applied, as shown in Fig. 4. The shapes agree very well, and show the forward peaking characteristic of beam-related backgrounds. The jaggedness of the $\cos\theta_\gamma$ plots results from the previously mentioned position dependence of our calorimeter trigger efficiency, which favors showers at the center and away from the edges of a trigger block.

In the high photon energy region ($E_\gamma > 1.5$ GeV), the event count is sufficiently low after application of cuts that visual scanning of individual events can be done to reject backgrounds. The events passing the cuts up to this point are independently scanned by three physicists. Events containing evidence of excess tracks or showers not detected by our off-line software are then flagged as likely background. All events which are classified as background by at least two of the three physicists are rejected from futher consideration. Of the 248 events with E_γ >1.5 GeV, 113 were rejected in scanning [20].

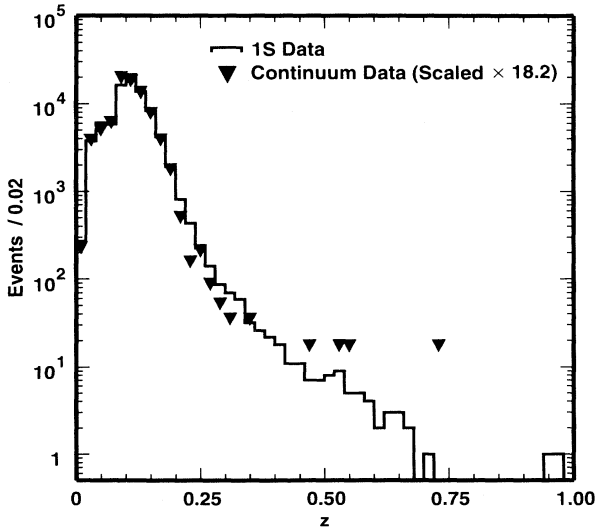

FIG. 3. $z(= E_\gamma/E_{\rm beam})$ in single-photon trigger events after applying all cuts. Note that the continuum has been scaled by a factor of 18.2.

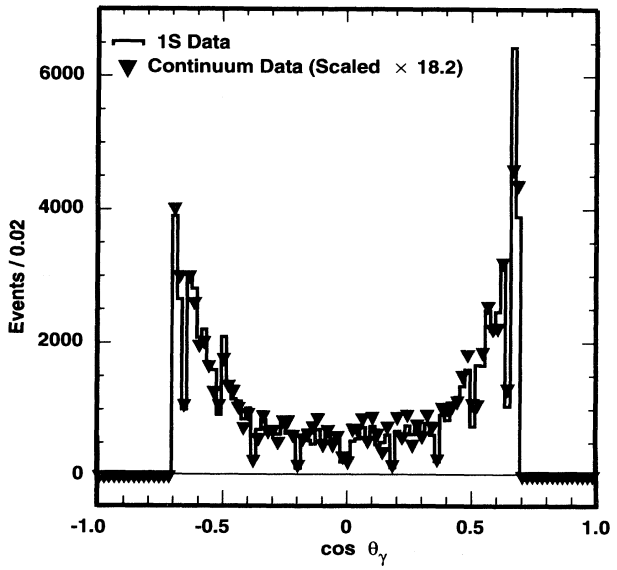

FIG. 4. $\cos\theta_\gamma$ of candidate photons after applying on-line and off-line photon selection cuts.

IV. OBTAINING UPPER LIMITS

A. Upper limit for $\Upsilon(1S) \rightarrow \gamma X$

1. High photon energies: $E_\gamma > 1.5$ GeV

After scanning, we are left with 135 real single-photon event candidates in the interval 1.5–4.7 GeV. The energy distribution of these events is displayed in Fig. 5.

We consider all these events as single-photon event candidates. No peaks are observed in the photon energy spectrum; the following procedure is followed to obtain upper limits for the two-body decay. For each mass hypothesis, we perform a maximum likelihood fit to a signal Gaussian (with a width fixed to that expected for a single photon in the CLEO-II CsI calorimeter) on top of a smooth low-order polynomial background. We use the fitted areas to determine upper limits on the branching ratios. The 90% C.L. upper limit at each photon energy was obtained by using the area of the fitted Gaussian (taken to be zero if negative) and the uncertainty in that fitted area using the Particle Data Group prescription [3] for probabilities that have physical bounds. For E_γ >2.68 GeV, we simply map the number of events within $\pm 2\sigma$ of the peak bin to a 90% confidence level upper limit; i.e., we assume all events are possible signal. Here, σ is the energy-dependent resolution on the reconstructed shower energy E_γ.

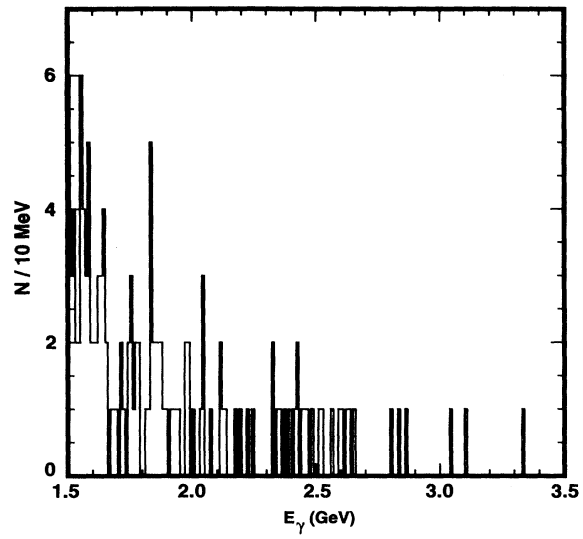

FIG. 5. E_γ distribution of photon candidates ($E_\gamma > 1.5$ GeV) surviving hardware and software cuts and physicist scanning as described in the text.

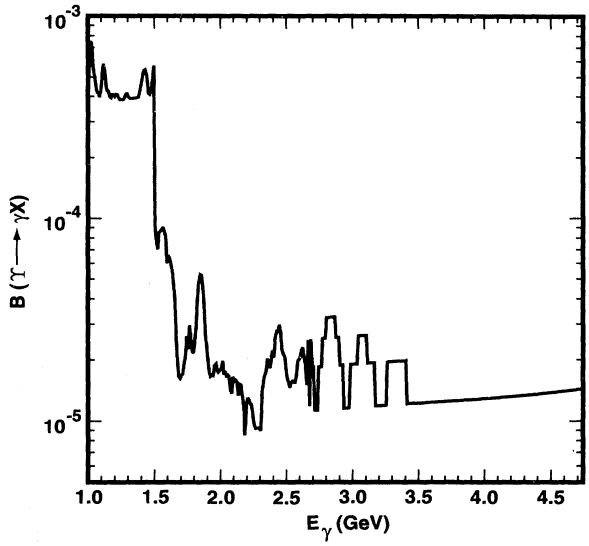

FIG. 7. 90% C.L. branching ratio for $\Upsilon(1S) \rightarrow \gamma X$ as a function of photon energy (LNS 1600894-008).

2. *Lower photon energies: $1.0 < E_\gamma < 1.5$ GeV*

Since the raw background shape does not fit a smooth polynomial in this region very well, it is more difficult to fit the raw data to a simple signal plus smooth background in the lower energy regime. For these events, we therefore perform the subtraction as outlined above, using the appropriately scaled continuum data as described previously. After the subtraction, we perform a bin-by-bin χ^2 fit to a Gaussian signal plus lower-order polynomial background, similar to the procedure for the higher energy data sample. Figure 6 displays a typical fit to the data.

Figure 7 shows a plot of our upper limit for the process $\Upsilon(1S) \rightarrow \gamma + X$, where X is any noninteracting particle, as a function of photon energy over the entire region for which we have sensitivity. Systematic errors have been incorporated here into our upper limit by recalculating the limit using a 1σ downward excursion in our calculated efficiency, taking into account the momentum dependence of this efficiency function. The systematic error is dominated by our uncertainty in the function $F(E_\gamma)$ (2% absolute), and our uncertainty in the off-line software filter (5% relative). There is an additional error of 4% which we calculate for our total number of $\Upsilon(1S)$ events (960 000).

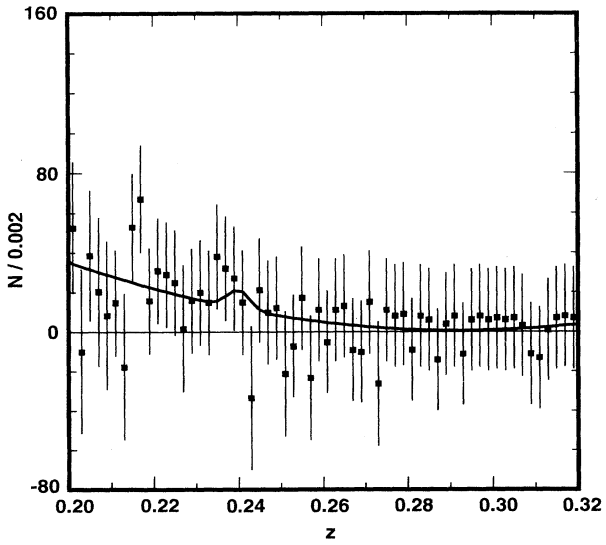

FIG. 6. Typical fit of background-subtracted candidate photon energy spectrum in the lower photon energy region to a Gaussian signal with the CLEO-II photon resolution plus a polynomial background function.

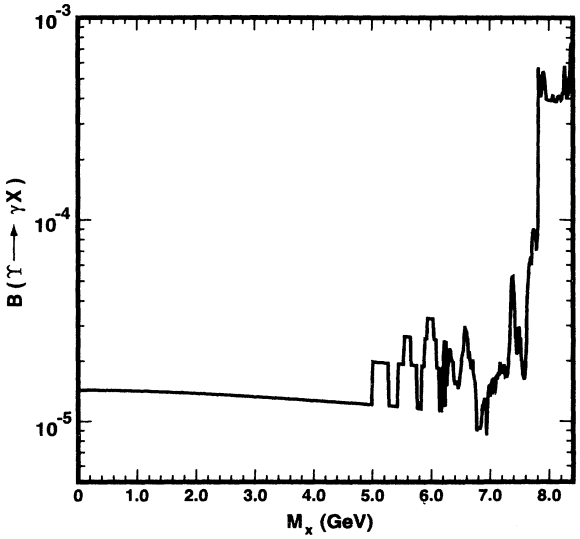

FIG. 8. 90% C.L. branching ratio for $\Upsilon(1S) \rightarrow \gamma X$ as a function of X mass, assuming X is a top pseudoscalar (LNS 1600894-009).

For the calculation of the upper limits, we have assumed that the particle X is a pseudoscalar, corresponding to a photon angular distribution of $1+\cos^2\theta$ relative to the beam axis. Our fiducial acceptance under this assumption is 0.61. The CLEO-II limit shown in Fig. 7 represents an improvement of the Crystal Ball's limit on the branching ratio of $\leq 5.6 \times 10^{-5}$ [1] over the interval 2.0–4.7 GeV. This is primarily the result of an increased sample size of $\Upsilon(1S)$ events relative to the Crystal Ball data set. Figure 8 displays the same upper limit as a function of X mass.

B. Upper limit for $\Upsilon(1S) \to \gamma \bar{X} X$

We use the scanned event sample only (higher photon energy) to determine the upper limit for a three-body decay. In principle, we could follow the same procedure as before by fitting to a signal shape plus a smooth background. Unlike the two-body case, however, for which the true photon energy for a given M_X would be monochromatic, here there is a range of energies that the photon can have in the interval $0 < E_\gamma < \left(\frac{M_\Upsilon^2}{2} - \frac{2M_X^2}{M_\Upsilon}\right)$. One could then generate a phase space spectrum for the photon energies, given a value of M_X and fit the observed data to a sum of that generated phase space spectrum (smeared by experimental resolution, as with the two-body case) plus a smooth background.

A more conservative limit is obtained by assuming all observed events are possible signal and calculating upper limits based on just these observed events. The spectrum observed from the continuum data, which matches the spectrum from the $\Upsilon(1S)$ data very well, as shown in Fig. 3, grows exponentially with decreasing photon energy. For a given value of M_X, we therefore restrict our E_γ interval to a region $E_\gamma > E_\gamma^{\min}(M_X)$. The minimum photon energy cut $E_\gamma^{\min}$ as a function of M_X is determined according to the following prescription: for each value of M_X, we generate the corresponding photon energy spectrum expected for a phase space three-body decay. The angular acceptance is calculated assuming a spin-1 object, for which the angular distribution as a function of photon momentum has been calculated [21], and is equivalent to the angular distribution of a direct photon in, e.g., $\Upsilon(1S) \to gg\gamma$. We then empirically determine a minimum photon energy cut $E_\gamma^{\min}(M_X)$ which gives the maximum sensitivity to the phase space decay of interest, as a function of X mass. This maximum sensitivity criterion for $E_\gamma^{\min}$ is defined as selecting that cut which optimizes the value of S^2/B, where S is the fraction of signal retained above $E_\gamma^{\min}$, and B is the amount of background filtering through for our exponentially falling background spectrum, as determined using our off-resonance data sample. We retain events for which $E_\gamma > E_\gamma^{\min}(M_X)$. For each value of M_X, we then summed the number of photons in our spectrum from this empirically determined cut up to the appropriate kinematic limit. Taking into account the photon-finding efficiency, along with the fraction of signal we retain, this sum is then mapped to a 90% confidence level upper limit.

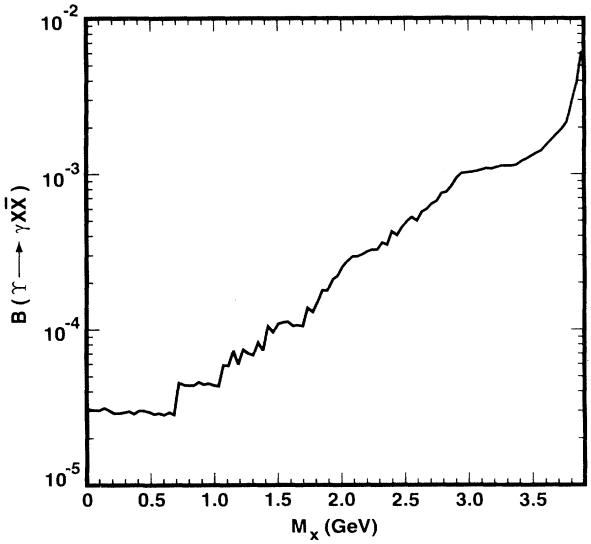

FIG. 9. 90% C.L. upper limit to the branching ratio for $\Upsilon(1S) \to \gamma X \bar{X}$, assuming the decay proceeds via three-body phase space, and assuming that X is a vectorially coupled particle. In the region between 1.0 and 3.0 GeV, the data approximately fit the form $B(\Upsilon(1S) \to \gamma X \bar{X}) < 10^{-5} \times \exp(1.54 M_X)$ at 90% C.L. (LNS 1600894-007).

Figure 9 shows our 90% confidence level upper limit on the branching ratio for the three-body decay, with systematic errors folded into the upper limit as outlined for the two-body case. We obtain upper limits on branching ratios in the range 10^{-5}–10^{-3} for $0 < M_X < 3.1$ GeV; above 3.1 GeV our limit on the branching ratio climbs steeply because of the poor efficiency for these values of M_X to produce a photon with energies above our minimum photon energy cut.

V. CONCLUSIONS

Using a sample of approximately one million $\Upsilon(1S)$ decays, we have searched for weakly interacting particles coupling to $b\bar{b}$ quarkonia. For two-body radiative decays of the $\Upsilon(1S)$ into a photon plus some undetected particle, we improved by a factor of two limits set by the Crystal Ball Collaboration. For three-body decays of the $\Upsilon(1S)$ resonance into a photon plus some undetected particle X and its antiparticle $\bar{X}$, we are sensitive at the 10^{-3} branching ratio level, and set upper limits as a function of the mass of the particle X. We find no evidence for nonstandard model couplings to bottomonia. If we interpret these results in the context of the "extra" U(1) gauge boson model, we determine that the U(1) symmetry-breaking energy scale should be at least of the order of twice the electroweak scale.

ACKNOWLEDGMENTS

We gratefully acknowledge the effort of the CESR staff in providing us with excellent luminosity and running conditions. This work was supported by the National Science Foundation and the U.S. Department of Energy. We also thank Pierre Fayet for illuminating discussions.

[1] Crystal Ball Collaboration, D. Antreasyan *et al.*, Phys. Lett. B **251**, 204 (1990).
[2] ARGUS Collaboration, H. Albrecht *et al.*, Z. Phys. C **42**, 349 (1989).
[3] Particle Data Group, K. Hikasa *et al.*, Phys. Rev. D **45**, S 1 (1992).
[4] R.D. Peccei and H.R. Quinn, Phys. Rev. Lett. **38**, 1440 (1977); Phys. Rev. D **16**, 1791 (1977).
[5] "Cosmion" is a generic term referring to a particle residing in the solar interior that can act as a heat sink and thus lower the temperature of the solar interior sufficiently so as to decrease significantly the production rate of ^{8}B neutrinos. It should be noted here that recent analyses of the combined Kamiokande and Homestake results mutually exclude core temperature depression as a candidate for the reduced observed neutrino flux, within the context of the standard solar model.
[6] P. Fayet and J. Kaplan, Phys. Lett. B **269**, 213 (1991).
[7] M. Cakir and G. Farrar, Phys. Rev. D **50**, 3268 (1994).
[8] C. Edwards *et al.*, Phys. Rev. Lett. **48**, 903 (1982).
[9] P. Fayet, Phys. Lett. **95B**, 285 (1980); Nucl. Phys. **B347**, 743 (1990); *ibid.* **B187**, 184 (1981); P. Fayet and M. Mezard, Phys. Lett. **104B**, 226 (1981); P. Fayet, *ibid.* **84B**, 421 (1979).
[10] P. Fayet, "New Interactions and the Standard Models," invited talk given at the Satellite Test of the Equivalence Principle symposium, Pisa, 1993, Report No. LPTENS 93-24 (unpublished).
[11] We implicitly assume for this paper that the undetected particles being searched for are "stable" in that they would not decay within the volume of the CLEO detector.
[12] Y. Kubota *et al.*, Nucl. Instrum. Methods Phys. Res. Sect. A **320**, 66 (1992).
[13] The quoted efficiencies are for an individual cut applied to, e.g., the $e^+e^- \to \gamma\gamma$ sample, and do not include correlations between cuts.
[14] CLEO has two track processors with input to the trigger decision. Both are here required to have zero for these inputs. One, which measures the scalar transverse momenta of tracks, would have nonzero inputs at the level of 90 MeV/c; the other, which finds track segments, would have nonzero inputs if one track traversed the entire chamber or if two tracks went halfway through it.
[15] Since this function $F(E_\gamma)$ is determined taking into account correlations between this efficiency and the other sources of inefficiency; the net efficiency is the product of this curve and the previously tabulated efficiencies.
[16] This follows from the relation $M_X^2 = M_\Upsilon^2 - 2M_\Upsilon E_\gamma$, appropriate for a two-body radiative Υ decay. From this expression, the Crystal Ball minimum energy cut of 2 GeV therefore corresponds to a sensitivity in mass extending up to $M_X \leq 7.2$ GeV.
[17] The failure of these events, which generally contain real charged tracks, to register tracking information in the central drift chamber is due to the fact that an event which has had a trigger initiated in the calorimeter reads out data in the drift chamber which is stale. This happens in a very small fraction of those events with real charged tracks ($<<1\%$).
[18] The off-resonance data corresponded to 4.86 pb^{-1}, compared with 48.2 pb^{-1} of on-resonance data. If the backgrounds are all single beam, then the magnitude of the background should scale with specific luminosity. The specific luminosity on the $\Upsilon(1S)$ is 0.60 (A h)/pb^{-1}; at the continuum energies, this value is 0.33 (A h)/pb^{-1}. The expected scale factor is then $\frac{(48.2)\times(0.60)}{(4.86)\times(0.33)} \sim 18.0$, in good agreement with the scale factor we derive empirically.
[19] We have considered two possible normalization schemes to determine the continuum scale factor—the first matches the continuum z spectrum to the $\Upsilon(1S)$ sample by normalizing by area, the second determines the scale factor by performing a χ^2 fit. The scale factor that we determine varies by 2%, depending on the choice of normalization. For the former case, the normalization factor obtained is 18.2. When determining final upper limits, we take the mean of the upper limits calculated using the two normalizations separately, and include the difference between them in the systematic error.
[20] We assess the inefficiency incurred in this scanning procedure by scanning Monte Carlo events into which noise and other effects not related to e^+e^- annihilation have been embedded. The scanning efficiency is estimated by this procedure to be 91%.
[21] K. Koller and T. Walsh, Nucl. Phys. **B140**, 449 (1978).